Letter

Topological spin texture and d-vector rotation in spin-triplet superconductors: A case of UTe_2

Yasumasa Tsutsumi
Department of Physics, Kwansei Gakuin University, Sanda, Hyogo 669-1330, Japan

Kazushige Machida
Department of Physics, Ritsumeikan University, Kusatsu 525-8577, Japan

(Received 3 October 2023; revised 22 July 2024; accepted 24 July 2024; published 9 August 2024)

A novel spin texture formed by Cooper pair spins is found theoretically with a phase string attached by half-quantized vortices at both ends in a unit cell and characterized by its topologically rich vortex structure in a spin-triplet pairing. It is stable at an intermediate field below a conventional singular vortex phase. The d-vector direction of this spin texture is tilted from the principal crystal axes, whose spin susceptibility is neither the normal Pauli one χ_N nor zero, describing microscopically the process of the d-vector rotation phenomena observed recently in UTe_2. We compare the spin texture and singular vortex state in relation to the quasiparticle structure with Majorana zero modes for STM, the nuclear spin resonance spectral line width for NMR and μSR, and the vortex form factors for SANS to facilitate the identification of the pairing symmetry in UTe_2.

DOI: 10.1103/PhysRevB.110.L060507

A spin-triplet pairing is extremely rare in nature. However, its utility is highly envisioned in fundamental physics to applications such as quantum computation, except for superfluid ^{3}He [1–3]. Only a few phases have been identified among the rich ($3 \times 3 \times 2 = 18$)-dimensional order parameter space spanned by $SO(3)_{spin} \times SO(3)_{orbital} \times U(1)_{gauge}$ such as ABM and BW, or more recently, their distorted versions in addition to the polar [4] and β phases [5]. In this context, the pairing symmetry in a prime candidate of a spin-triplet pairing of UTe_2 as a solid-state counterpart is quite intriguing, and its identification is critical.

The concept of the d-vector rotation is well established in neutral ^{3}He superfluids [1–3]. The d vector, which fully characterizes a spin-triplet pairing, changes its direction uniformly in bulk under a magnetic field to minimize the Zeeman energy loss due to the Pauli paramagnetic effect acting on the Cooper pair spin. Namely, the d-vector tries to remain perpendicular to the field orientation because the anisotropic spin susceptibility parallel to $\vec{d}$ is smaller than that perpendicular to $\vec{d}$. In contrast, the situation is more complicated and physically richer for a spin-triplet superconductor with charged fermions because the applied field inevitably induces the depairing current acting on the Cooper pair orbital motion associated with vortices in addition to the Pauli effect. Thus, the d-vector rotation is realized by a vortex morphological change, or a spin textural change of Cooper pairs in general. Although experimental observations have been reported recently in UTe_2 [6–11] and UPt_3 [12,13] a long time ago, where the Knight shift gradually changes as varying a field, its microscopic description has not been done before. The experimental observations are interpreted only phenomenologically [14]. This task is crucial in identifying the pairing symmetry and topological nature of materials.

UTe_2 is a newly found heavy fermion superconductor [15] and is regarded as a spin-triplet pairing candidate. Currently, there is much attention focused on this strongly correlated system because of the following reasons: (i) The Knight shift (KS), or the spin susceptibility $\chi_s(T)$ decreases for all principal field directions, a, b, and c axes at lower H [6–11]. As a function of H, $\chi_s(H)$ becomes gradually unchanged for $H \parallel b$ and c axes at lower T. Thus, $\chi_s(H) = \chi_N$ with χ_N normal spin susceptibility. This is incompatible with the ^{3}He-B phaselike state because it simply means the loss of the condensation energy by eliminating the component parallel to the field direction. However, this is physically improbable. Moreover, the magnitude of the KS change for the a axis is abnormally larger (four times the normal susceptibility) than the other b and c directions [11], implying that KS for the $H \parallel a$ axis is governed by a mechanism different from the ordinary KS drop, rather analogous to the Takagi mechanism observed in ^{3}He-A phase [16]. (ii) The H-T phase diagram for the $H \parallel b$ axis, which is the main focus of the present study, consists of three phases [17–20]: low (LSC), intermediate (MSC), and high (HSC) field phases. They meet at a tetracritical point: $H_{tetra} \sim 15$ T. H_{c2} for HSC has a prominent positive slope $(dT_c/dH)_{H_{c2}} > 0$ emanating from H_{tetra}. KS remains unchanged (decreases) for HSC (LSC). MSC in 15 T $\lesssim H \lesssim$ 22 T is characterized by a finite flux flow state where vortices are highly mobile [18,19], suggesting that an exotic coreless vortex is formed [19]. Interestingly, it approximately corresponds to a field region in which $\chi_s(H)$ is varying toward χ_N and reaching at $H \sim 15$ T with increasing H. Under pressure, the phase diagram has more than three distinct phases [21,22]. (iii) There exists a variety of nontrivial superconducting properties. The polar Kerr experiment shows that SC breaks time-reversal symmetry [23]. The STM measurements detect the chiral symmetry-breaking state at sample edges [24] and pair-density wave [25]. Several thermodynamic experiments suggest a nodal gap structure [26–30]. H_{c2} for three crystal directions far exceeds the Pauli limiting field [26].

These experimental findings provide strong evidence for a spin-triplet pairing in UTe_2. The order parameter must be properly configured to describe the d-vector rotation phenomenon microscopically. Since $\chi_s(T)$ decreases below T_c for three principal directions at lower fields, the d vector must have three components with complex numbers whose transition temperatures associated with each component are nearly degenerate; otherwise, continuous d-vector rotation is impossible. Upon increasing the $H \parallel b(c)$ axis, $\chi_s(H)(<\chi_N)$ starts to gradually increase toward χ_N at approximately 5 T (1 T), and finally reaches χ_N at approximately $H^b_{\rm rot} = 15$ T ($H^c_{\rm rot} = 5$ T). Since $H^i_{\rm rot}$ ($i = b, c$) depends on the field orientations, those are slightly different, reflecting that the original spin space symmetry $\mathrm{SO(3)_{spin}}$ is weakly broken [31–36]. We ignore this weak symmetry breaking to investigate the generic features of the stable spin texture and establish the concept of the d-vector rotation in the following.

The purpose of this study is to find a stable spin texture in a spin-triplet pairing under $\mathrm{SO(3)_{spin}}$ symmetry, by solving the microscopic quasiclassical Eilenberger equation for a spin-triplet pairing [37] with full three components of the order parameter. This turns out to be rich topological features with Majorana zero modes. We also establish the concept of the d-vector rotation in connection with $\mathrm{UTe_2}$. In particular, the recently found MSC for $H \parallel b$ with mobile vortices is explained in terms of the above spin texture consisting of coreless vortices.

We can obtain physical quantities from the quasiclassical Green's function defined in the 4×4 matrix in particle-hole and spin spaces,

$$\widehat{g}(\boldsymbol{k},\boldsymbol{r},\omega_n) = -i\pi \begin{pmatrix} \hat{g}(\boldsymbol{k},\boldsymbol{r},\omega_n) & i\hat{f}(\boldsymbol{k},\boldsymbol{r},\omega_n) \\ -i\underline{\hat{f}}(\boldsymbol{k},\boldsymbol{r},\omega_n) & -\underline{\hat{g}}(\boldsymbol{k},\boldsymbol{r},\omega_n) \end{pmatrix}, \quad (1)$$

depending on the direction of the relative momentum of a Cooper pair $\boldsymbol{k}$, the center-of-mass coordinate of the Cooper pair $\boldsymbol{r}$, and the Matsubara frequency $\omega_n = (2n+1)\pi k_B T$. It satisfies the normalization condition $\widehat{g}^2 = -\pi^2\widehat{1}$. $\widehat{g}(\boldsymbol{k},\boldsymbol{r},\omega_n)$ is calculated using the Eilenberger equation [38–42],

$$-i\hbar\boldsymbol{v}(\boldsymbol{k})\cdot\nabla\widehat{g} = \left[\begin{pmatrix} \hat{K} - \mu_{\rm B}\boldsymbol{B}(\boldsymbol{r})\cdot\hat{\boldsymbol{\sigma}} & -\hat{\Delta}(\boldsymbol{k},\boldsymbol{r}) \\ \hat{\Delta}(\boldsymbol{k},\boldsymbol{r})^\dagger & -\hat{K} - \mu_{\rm B}\boldsymbol{B}(\boldsymbol{r})\cdot\hat{\boldsymbol{\sigma}}^* \end{pmatrix}, \widehat{g}\right], \quad (2)$$

where $\hat{K} \equiv \hat{K}(\boldsymbol{k},\boldsymbol{r},\omega_n) = [i\omega_n + e\boldsymbol{v}(\boldsymbol{k})\cdot\boldsymbol{A}(\boldsymbol{r})]\hat{1}$. It includes the paramagnetic effects due to the Zeeman term $\mu_{\rm B}\boldsymbol{B}(\boldsymbol{r})\cdot\hat{\boldsymbol{\sigma}}$, where $\mu_{\rm B}$ is a renormalized Bohr magneton, $\boldsymbol{B}(\boldsymbol{r})$ is the flux density of the internal field, and $\hat{\boldsymbol{\sigma}}$ is the Pauli matrix. In this study, we consider the two-dimensional cylindrical Fermi surface, $\boldsymbol{k} = k_{\rm F}(\cos\theta, \sin\theta)$, with the Fermi velocity $\boldsymbol{v}(\boldsymbol{k}) = v_{\rm F}(\cos\theta, \sin\theta)$, where $0 \leqslant \theta < 2\pi$.

We assume the chiral p-wave pairing symmetry with the pairing function $\phi(\boldsymbol{k}) = e^{i\theta}$ independent of the spin state. In the assumption, the spin-triplet order parameter is given by $\hat{\Delta}(\boldsymbol{k},\boldsymbol{r}) = i\phi(\boldsymbol{k})\boldsymbol{d}(\boldsymbol{r})\cdot\hat{\boldsymbol{\sigma}}\hat{\sigma}_y$, with the local d vector $\boldsymbol{d}(\boldsymbol{r})$. The self-consistent condition for $\hat{\Delta}(\boldsymbol{k},\boldsymbol{r})$ is given as $\hat{\Delta}(\boldsymbol{k},\boldsymbol{r}) = N_0\pi k_B T\sum_{|\omega_n|\leqslant\omega_c}\langle V(\boldsymbol{k},\boldsymbol{k}')\hat{f}(\boldsymbol{k}',\boldsymbol{r},\omega_n)\rangle_{\boldsymbol{k}'}$ where N_0 is the density of states (DOS) in the normal state, ω_c is the cutoff energy setting $\omega_c = 20\pi k_B T_c$ with the transition temperature T_c, and $\langle\cdots\rangle_{\boldsymbol{k}}$ indicates the Fermi surface average. The pairing interaction $V(\boldsymbol{k},\boldsymbol{k}') = g\phi(\boldsymbol{k})\phi^*(\boldsymbol{k}')$, where g is a coupling constant.

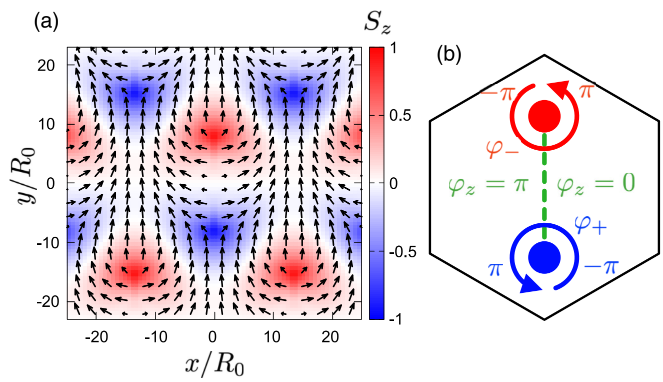

FIG. 1. (a) Spin texture $\boldsymbol{S} = i(\boldsymbol{d}\times\boldsymbol{d}^*)/|\boldsymbol{d}|^2$ with $\bar{B} = 0.01B_0$, $\mu = 1$, and $T = 0.2T_c$. (b) Schematic picture for phases of d-vector components in a unit cell of the hexagonal vortex lattice. The green dotted line indicates the phase string across which the phase of d_z jumps by π. Both ends, indicated by red and blue dots, correspond to the half-quantized vortices.

In our calculation, we use the relation $1/gN_0 = \ln(T/T_c) + \pi k_B T\sum_{|\omega_n|\leqslant\omega_c} 1/|\omega_n|$.

The vector potential $\boldsymbol{A}(\boldsymbol{r})$ is determined by

$$\frac{R_0}{B_0}\nabla\times[\nabla\times\boldsymbol{A}(\boldsymbol{r})] = \frac{R_0}{B_0}\nabla\times\boldsymbol{M}_{\rm para}(\boldsymbol{r}) + i\frac{1}{\kappa^2}\frac{T}{T_c}\sum_{|\omega_n|\leqslant\omega_c}\left\langle\frac{\boldsymbol{k}}{k_{\rm F}}g_0(\boldsymbol{k},\boldsymbol{r},\omega_n)\right\rangle_{\boldsymbol{k}}, \quad (3)$$

where g_0 is a component of the quasiclassical Green's function $\hat{g}$ in spin space, namely, $\hat{g} = g_0\hat{1} + \boldsymbol{g}\cdot\hat{\boldsymbol{\sigma}}$. Here, we show the dimensionless expression with the units $R_0 = \hbar v_F/(2\pi k_B T_c)$, $B_0 = \hbar/(2|e|R_0^2)$, $\kappa = B_0/(E_0\sqrt{2N_0}) = \sqrt{7\zeta(3)/8}\kappa_{\rm GL}$, and $E_0 = \pi k_B T_c$. We use a large Ginzburg–Landau (GL) parameter $\kappa_{\rm GL} = 60$. The paramagnetic moment is given by

$$\boldsymbol{M}_{\rm para}(\boldsymbol{r}) = \boldsymbol{M}_0(\boldsymbol{r}) + i\frac{\mu B_0}{\kappa^2}\frac{T}{T_c}\sum_{|\omega_n|\leqslant\omega_c}\langle\boldsymbol{g}(\boldsymbol{k},\boldsymbol{r},\omega_n)\rangle_{\boldsymbol{k}}, \quad (4)$$

with $\mu = \mu_{\rm B}B_0/E_0$ and the normal-state paramagnetic moment $\boldsymbol{M}_0(\boldsymbol{r}) = 2\mu_{\rm B}^2 N_0\boldsymbol{B}(\boldsymbol{r})$. We obtain a self-consistent solution under a given unit cell of the vortex lattice by a uniform flux density $\bar{\boldsymbol{B}} = (0, 0, \bar{B})$ [43–47] (see the detail in Supplemental Material [48]).

Local spin polarization of the Cooper pair is given by the local d vector as $\boldsymbol{S}(\boldsymbol{r}) = i[\boldsymbol{d}(\boldsymbol{r})\times\boldsymbol{d}(\boldsymbol{r})^*]/|\boldsymbol{d}(\boldsymbol{r})|^2$ [49]. We obtain a stable spin texture by the self-consistent calculation. The spin texture under the magnetic field $\bar{B} = 0.01B_0$ with $\mu = 1$ at $T = 0.2T_c$ is shown in Fig. 1. The area of the unit cell of the hexagonal vortex lattice is $200\pi R_0^2$ under this magnetic field. The spin texture has a position with $S_z = +1$ and a position with $S_z = -1$ in the unit cell. The positions correspond to the phase singularity of d-vector components, $d_z = |d_z|e^{i\varphi_z}$ and $d_\pm = (\mp d_x + id_y)/\sqrt{2} = |d_\pm|e^{i\varphi_\pm}$.

A schematic picture for the phases, φ_z and $\varphi_\pm$, in a unit cell is shown in Fig. 1(b). The singularities of φ_+ and φ_- with 2π-phase winding are situated at $(0, -y_c)$ and $(0, +y_c)$, respectively, with $y_c \approx 5.6R_0$. Phase φ_z has singularities with

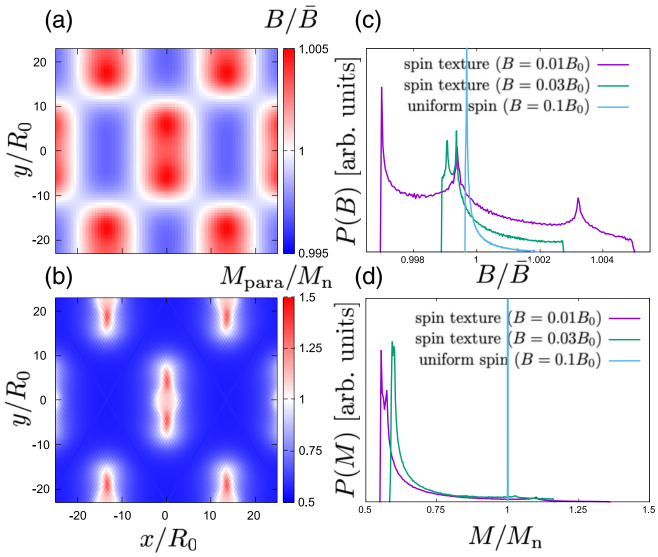

FIG. 2. (a) Spatial variations of internal field $B(\boldsymbol{r})$ and (b) paramagnetic moment $M_{\rm para}(\boldsymbol{r})$ with $\bar{B} = 0.01B_0$, $\mu = 1$, and $T = 0.2T_{\rm c}$. (c) Distributions of internal field $P(B)$ and (d) paramagnetic moment $P(M_{\rm para})$ with $\mu = 1$ and $T = 0.2T_{\rm c}$. The distributions are shown for spin textures under $\bar{B} = 0.01B_0$ and $\bar{B} = 0.03B_0$, and singular vortex structure with uniform spin parallel to the z axis under $\bar{B} = 0.1B_0$.

π-phase winding also at $(0, -y_{\rm c})$, and $(0, +y_{\rm c})$ and phase jumps by π at the branch cut on $x = 0$ connecting these two singularities. Thus, the phase of the d vector changes by 2π around the unit cell of the vortex lattice.

The phase singularities at $(0, \pm y_{\rm c})$ can be viewed as a half-quantized vortex (HQV) because locally $d_- e^{i\varphi_-} + d_+ = e^{i\varphi_-/2}\{d_x \cos(\varphi_-/2) + d_y \sin(\varphi_-/2)\}$. Therefore, the spin texture obtained is described as the two HQVs [red and blue dots in Fig. 1(b)] bound together by the string or branch cut (dotted green line) with the phase π jump. The amplitude of the order parameters in the spin texture is nonvanishing anywhere. As H increases, the string length decreases, and the objects merge to form a singular vortex. We can calculate the average d-vector direction over the unit cell, finding the tilting angle $10.6^\circ(11.3^\circ)$ for $\bar{B} = 0.01(0.03)B_0$ away from the xy plane.

The local spin of the Cooper pair is polarized in the $+y$ direction perpendicular to the field direction z on the boundary edge of the hexagonal unit cell shown in Fig. 1(b). In contrast, the d vector at (0,0) is parallel to the y axis with $\boldsymbol{S} = \boldsymbol{0}$. The spin polarization is shrunk around (0,0) with $|\boldsymbol{S}| < 1$. Note that $\Delta(\boldsymbol{r})$ is nonvanishing everywhere, as displayed in Fig. S1(a) [48]. Thus, this spin texture is coreless with the soft cores, which is contrasted with the singular vortex states, having the hard core, stabilized in higher fields (HSC) (see Supplemental Material for detail [48]). Note that the topological skyrmion number [50] for the spin polarization $\boldsymbol{S}(\boldsymbol{r})$ is ill defined due to $\boldsymbol{S}(\boldsymbol{0}) = \boldsymbol{0}$ [51]. Topological properties of the spin texture is discussed later in connection with the local density of states (LDOS).

Internal magnetic field $B(\boldsymbol{r})$ for the spin texture are shown in Fig. 2(a). The internal field has maxima at the positions of the phase singularity; namely, the spin of the Cooper pair is polarized to the z axis. As shown in Fig. 2(a), the central maximum region is thus elongated along the polarization direction of the y axis. The spatial dependence of the internal field gives the characteristic distribution function $P(B) \equiv \int \delta(B - B(\boldsymbol{r}))d\boldsymbol{r}$, whose intensity originates from the length of a contour satisfying $B = B(\boldsymbol{r})$. $P(B)$ for the spin texture under $\bar{B} = 0.01B_0$ has three peaks as shown in Fig. 2(c). The right peak around $B = 1.003\bar{B}$ originates from a contour enclosing each maximum of the internal field. The central peak slightly below $B = \bar{B}$ originates from the square contour colored with white in Fig. 2(a). The left peak at the lowest B comes from the minima of the internal field. In contrast, $P(B)$ for the singular vortex structure with uniform spin has a single peak due to internal field minima, as shown in Fig. 2(c). Thus $P(B)$ for the spin texture is more widely distributed than that for the singular vortex structure. The right peak at the highest B in the distribution function for the spin texture disappears under $\bar{B} = 0.03B_0$. This is because contours enclosing each maximum of the internal field become short owing to the maxima overlapping each other in the small area of the unit cell of the vortex lattice.

These remarkable three-peak structures in $P(B)$ can be observable by the muon spin rotation (μSR) experiment [52]. This significantly impacts the SANS experiment, as fundamental form factors [46] such as F_{10} and F_{20} increase as H increases, in sharp contrast to conventional SC, where these decrease exponentially with H [46,47] because the two singularities approach each other. Thus, the elongated high field region in Fig. 2(a) becomes round to concentrate it, causing those form factors to grow.

The paramagnetic moment $M_{\rm para}(\boldsymbol{r})$ shown in Fig. 2(b) also has maxima at the positions of the phase singularity similar to $B(\boldsymbol{r})$ mentioned above. However, it is more strongly confined near the phase singularities, as shown from Fig. 2(b). $M_{\rm para}(\boldsymbol{r})$ approaches $M_{\rm n}/2$ on the edge of the hexagonal unit cell because one of two components of the d vector parallel to the x and z axes is parallel to the magnetic field. The distribution functions of $M_{\rm para}(\boldsymbol{r})$, $P(M) \equiv \int \delta(M - M_{\rm para}(\boldsymbol{r}))d\boldsymbol{r}$, for the spin texture and the singular vortex structure are shown in Fig. 2(d). $P(M)$ for the spin texture has double peaks in low M compared to the singular vortex structure case. The double peaks originates from long contours enclosing the minima of the paramagnetic moment compared to the sharp single peak in the singular vortex.

$P(M)$ is directly measured by NMR on ^{125}Te as KS [7]. The gradual change of KS with field for the $H \parallel b$ axis is interpreted as the d-vector rotation [7,8]. Here, we have shown theoretically that this is indeed the case: Starting at the lower field for LSC with $\chi_{\rm s} = \chi_{\rm N}/2$ where all the d vectors are parallel to z, the peak position moves up from $M = M_{\rm n}/2$ with increasing H as shown in Fig. 2(d). During this process, the d vector rotates away from the field direction in MSC. The average d-vector direction over a unit cell for the spin texture is tilted away from the field direction. The shift of the peak position of $P(M)$ precisely corresponds to the d-vector angle away from $\boldsymbol{B}$. This process of the spin textural changes continues until all the local spin polarizations $\boldsymbol{S}(\boldsymbol{r})$ direct along $\boldsymbol{B}$ with the peak at $M = M_{\rm n}$. At higher fields $P(M)$ has a single sharp peak at the normal state position: $M = M_{\rm n}$ as shown in Fig. 2(d), corresponding to HSC, with all the d vectors perpendicular to z. The resulting vortex has a singularity at the vortex core, bearing the genuine Majorana zero mode,

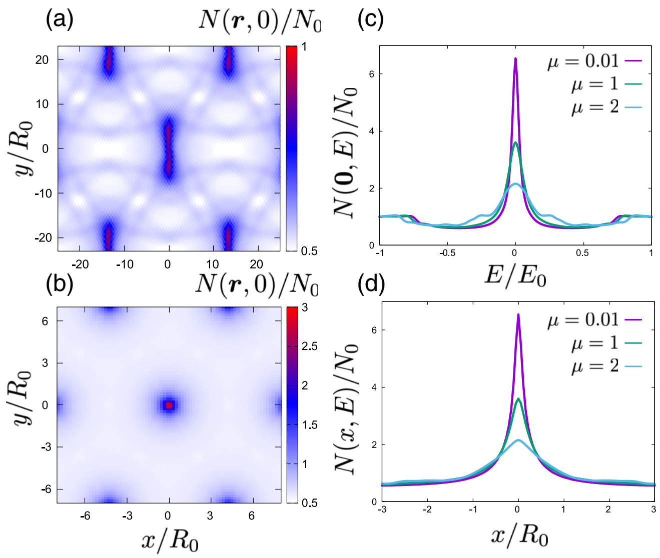

FIG. 3. (a) Zero-energy LDOS for the spin texture under $\bar{B} = 0.01B_0$ and (b) singular vortex structure with uniform spin parallel to the y axis under $\bar{B} = 0.1B_0$ with $\mu = 1$ and $T = 0.2T_c$. (c) Energy profiles of the LDOS $N(\mathbf{0}, E)$ at the vortex core and (d) spatial variations of the zero energy LDOS $N(x, 0)$ along the x axis for the singular vortex structure with $\mu = 0.01$, $\mu = 1$, and $\mu = 2$.

as explained in Supplemental Material [48]. The one-to-one correspondence between the tilting angle and the peak position deviation from the bottom at $M_n/2$ in KS establishes the concept of the d-vector rotation phenomenon.

The LDOS for the energy E is given by $N_\sigma(\boldsymbol{r}, E) = N_0\langle \mathrm{Re}[g_0(\boldsymbol{k}, \boldsymbol{r}, \omega_n)|_{i\omega_n\to E+i\eta}]\rangle_{\boldsymbol{k}}$, where η is a positive infinitesimal constant assigned $\eta = 0.03E_0$ in this paper. The zero-energy LDOS for the spin texture with $\bar{B} = 0.01B_0$, $\mu = 1$, and $T = 0.2T_c$ is shown in Fig. 3(a). The zero-energy quasiparticles are localized in the phase singularity of d-vector components $d_\pm$, and their LDOS extends along the branch cut, or phase string attached to the two singularities at both ends across which the phase of d_z jumps by π. Each of the localized modes is single Majorana zero-energy mode protected by the symmetry of the magnetic reflection on the plane including the brunch cut of d_z. The magnetic reflection symmetry gives the one-dimensional winding number in the mirror-symmetric subspace. The change of the winding number at the singularities of $d_\pm$, which guarantees the existence of the single zero-energy mode localized in the singularities (see the detail in Supplemental Material [48]).

In contrast, the zero-energy quasiparticles are concentrated in the vortex core for the singular vortex structure. The concentration of the zero-energy LDOS is clearly shown in Fig. 3(b) for the singular vortex structure with $\boldsymbol{S} \parallel \boldsymbol{y}$ under $\bar{B} = 0.1B_0$ at $T = 0.2T_c$ with $\mu = 1$. The dependence of the LDOS on the strength of the Pauli paramagnetic effect, μ, is found in the energy profile of the LDOS at the vortex core [Fig. 3(c)] and the spatial variation of the zero-energy LDOS along the x axis [Fig. 3(d)]. The intensity of the zero-energy LDOS at the vortex core decreases as the Pauli paramagnetic effect increases. The suppression of the zero-energy peak height is accompanied by the broadening of the low-energy spectrum, as shown in Fig. 3(c). A spatial spread of the zero-energy LDOS around the vortex core is less sensitive to the strength of the Pauli paramagnetic effect [Fig. 3(d)]. In contrast, the Pauli paramagnetic effect does not affect the LDOS for the singular vortex structure with $\boldsymbol{S} \parallel \boldsymbol{z}$. Then, the LDOS for the singular vortex with $\boldsymbol{S} \parallel \boldsymbol{z}$ is equivalent to that with $\boldsymbol{S} \parallel \boldsymbol{y}$ for $\mu = 0$. Note that the LDOS is larger than $N_0/2$ because one of the spin states remains in the normal state in the spin-polarized superconductivity.

A singular vortex with $\boldsymbol{S} \parallel \boldsymbol{z}$ in HSC has a spin-polarized Majorana zero-energy mode [53] regardless of the Pauli paramagnetic effect. The Pauli paramagnetic effect hybridizes a spin-polarized zero-energy mode in the vortex core with quasiparticles in the normal spin state for a singular vortex with $\boldsymbol{S} \parallel \boldsymbol{y}$. Despite the hybridization of the spin states, their energy levels do not shift from zero energy. The zero-energy modes in a singular vortex with $\boldsymbol{S} \parallel \boldsymbol{y}$ are protected by the magnetic reflection symmetry similarly to the zero modes in the spin texture (see the detail in Supplemental Material [48]).

In summary, we microscopically described the d-vector rotation phenomena by solving the Eilenberger equation for a spin-triplet pairing to understand this concept. The obtained spin texture $\boldsymbol{S}(\boldsymbol{r})$ for MSC stabilized below the singular vortex state with uniform $\boldsymbol{S} \parallel \boldsymbol{B}$ for HSC was fully characterized, providing several important indications to understand experimental data on UTe_2. Table I summarizes the characteristics of the three phases. In particular, the newly found MSC experimentally characterized by an unusual flux flow state, or mobile vortices [18,19], might correspond to this spin texture, consisting of two coreless HQV's tagged by the phase string. We demonstrated the rich topological features, including the locations of the Majorana zero modes associated with the spin texture to be investigated experimentally in UTe_2.

K.M. thanks K. Ishida, S. Kitagawa, H. Sakai, D. Aoki, Y. Shimizu, S. Kittaka, T. Sakakibara, Y. Tokunaga, Y. Haga, and A. Miyake for helpful discussions. In particular, K. Ishida allowed us to share their unpublished data, which motivated the present project. This work was supported by JSPS KAKENHI, Projects No.17K05553, No. 21K03455, and No. 21K03456 and performed in part at Aspen Center for Physics, which is supported by National Science Foundation Grant No. PHY-2210452.

TABLE I. Characterizations of the three phases.

Phase	χ_s/χ_N	d vector	Core	Majorana modes	Width[a]
LSC	1/2	d $\parallel$ B (uniform)	–	–	–
MSC	$1/2 \sim 1$	spin texture	Soft	Each singularity	Wide
HSC	1	d $\perp$ B (uniform)	Hard	A singular core	Narrow

[a]width: NMR resonance width.

[1] G. E. Volovik, *The Universe in a Helium Droplet* (Oxford University Press, Oxford, 2002).

[2] D. Vollhart and P. Wölfle, *The Superfluid Phases of Helium 3* (Taylor and Francis, London, 1990).

[3] T. Mizushima, Y. Tsutsumi, T. Kawakami, M. Sato, M. Ichioka, and K. Machida, Symmetry-protected topological superfluids and superconductors—from the basics to ^{3}He—, J. Phys. Soc. Jpn. **85**, 022001 (2016).

[4] V. V. Dmitriev, A. A. Senin, A. A. Soldatov, and A. N. Yudin, Polar phase of superfluid ^{3}He in anisotropic aerogel, Phys. Rev. Lett. **115**, 165304 (2015).

[5] V. V. Dmitriev, M. S. Kutuzov, A. A. Soldatov, and A. N. Yudin, Superfluid β phase in liquid ^{3}He, Phys. Rev. Lett. **127**, 265301 (2021).

[6] G. Nakamine, S. Kitagawa, K. Ishida, Y. Tokunaga, H. Sakai, S. Kambe, A. Nakamura, Y. Shimizu, Y. Homma, D. Li, F. Honda, and D. Aoki, Superconducting properties of heavy fermion UTe_2 revealed by ^{125}Te-nuclear magnetic resonance, J. Phys. Soc. Jpn. **88**, 113703 (2019).

[7] G. Nakamine, K. Kinjo, S. Kitagawa, K. Ishida, Y. Tokunaga, H. Sakai, S. Kambe, A. Nakamura, Y. Shimizu, Y. Homma, D. Li, F. Honda, and D. Aoki, Inhomogeneous superconducting state probed by ^{125}Te NMR on UTe_2, J. Phys. Soc. Jpn. **90**, 064709 (2021).

[8] G. Nakamine, K. Kinjo, S. Kitagawa, K. Ishida, Y. Tokunaga, H. Sakai, S. Kambe, A. Nakamura, Y. Shimizu, Y. Homma, D. Li, F. Honda, and D. Aoki, Anisotropic response of spin susceptibility in the superconducting state of UTe_2 probed with ^{125}Te-NMR measurement, Phys. Rev. B **103**, L100503 (2021).

[9] H. Fujibayashi, G. Nakamine, K. Kinjo, S. Kitagawa, K. Ishida, Y. Tokunaga, H. Sakai, S. Kambe, A. Nakamura, Y. Shimizu, Y. Homma, D. Li, F. Honda, and D. Aoki, Superconducting order parameter in UTe_2 determined by Knight shift measurement, J. Phys. Soc. Jpn. **91**, 043705 (2022).

[10] K. Kinjo, H. Fujibayashi, S. Kitagawa, K. Ishida, Y. Tokunaga, H. Sakai, S. Kambe, A. Nakamura, Y. Shimizu, Y. Homma, D. X. Li, F. Honda, D. Aoki, K. Hiraki, M. Kimata, and T. Sasaki, Magnetic field-induced transition with spin rotation in the superconducting phase of UTe_2, Phys. Rev. B **107**, L060502 (2023).

[11] H. Matsumura, H. Fujibayashi, K. Kinjo, S. Kitagawa, K. Ishida, Y. Homma, D. Li, F. Honda, and D. Aoki, Large reduction in the a-axis Knight shift on UTe_2 with T_c=2.1K, J. Phys. Soc. Jpn. **92**, 063701 (2023).

[12] H. Tou, Y. Kitaoka, K. Asayama, N. Kimura, Y. Onuki, E. Yamamoto, and K. Maezawa, Odd-parity superconductivity with parallel spin pairing in UPt_3: Evidence from ^{195}Pt Knight shift study, Phys. Rev. Lett. **77**, 1374 (1996).

[13] H. Tou, Y. Kitaoka, K. Ishida, K. Asayama, N. Kimura, Y. Onuki, E. Yamamoto, Y. Haga, and K. Maezawa, Nonunitary spin-triplet superconductivity in UPt_3: Evidence from ^{195}Pt Knight shift study, Phys. Rev. Lett. **80**, 3129 (1998).

[14] K. Machida, T. Nishira, and T. Ohmi, Orbital symmetry of a triplet pairing in a heavy fermion superconductor UPt_3, J. Phys. Soc. Jpn. **68**, 3364 (1999).

[15] S. Ran, C. Eckberg, Q.-P. Ding, Y. Furukawa, T. Metz, S. R. Saha, I.-L. Liu, M. Zic, H. Kim, J. Paglione, and N. P. Butch, Nearly ferromagnetic spin-triplet superconductivity, Science **365**, 684 (2019).

[16] S. Takagi, Susceptibility discontinuity at the He^3-A-normal transition, Prog. Theor. Phys. **51**, 1998 (1974).

[17] G. Knebel, W. Knafo, A. Pourret, Q. Niu, M. Vališka, D. Braithwaite, G. Lapertot, M. Nardone, A. Zitouni, S. Mishra, I. Sheikin, G. Seyfarth, J.-P. Brison, D. Aoki, and J. Flouquet, Field-reentrant superconductivity close to a metamagnetic transition in the heavy-fermion superconductor UTe_2, J. Phys. Soc. Jpn. **88**, 063707 (2019).

[18] H. Sakai, Y. Tokiwa, P. Opletal, M. Kimata, S. Awaji, T. Sasaki, D. Aoki, S. Kambe, Y. Tokunaga, and Y. Haga, Field induced multiple superconducting phases in UTe_2 along hard magnetic axis, Phys. Rev. Lett. **130**, 196002 (2023).

[19] Y. Tokiwa, H. Sakai, S. Kambe, P. Opletal, E. Yamamoto, M. Kimata, S. Awaji, T. Sasaki, Y. Yanase, Y. Haga, and Y. Tokunaga, Anormalous vortex dynamics in spin-triplet superconductor in UTe_2, Phys. Rev. B **108**, 144502 (2021).

[20] A. Rosuel, C. Marcenat, G. Knebel, T. Klein, A. Pourret, N. Marquardt, Q. Niu, S. Rousseau, A. Demuer, G. Seyfarth, G. Lapertot, D. Aoki, D. Braithwaite, J. Flouquet, and J.-P. Brison, Field-induced tuning of the pairing state in a superconductor, Phys. Rev. X **13**, 011022 (2023).

[21] D. Braithwaite, M. Valiska, G. Knebel, G. Lapertot, J.-P. Brison, A. Pourret, M. E. Zhitomirsky, J. Flouquet, F. Honda, and D. Aoki, Multiple superconducting phases in a nearly ferromagnetic system, Commun. Phys. **2**, 147 (2019).

[22] D. Aoki, F. Honda, G. Knebel, D. Braithwaite, A. Nakamura, D. Li, Y. Homma, Y. Shimizu, Y. J. Sato, J.-P. Brison, and J. Flouquet, Multiple superconducting phases and unusual enhancement of the upper critical field in UTe_2, J. Phys. Soc. Jpn. **89**, 053705 (2020).

[23] D. S. Wei, D. Saykin, O. Y. Miller, S. Ran, S. R. Saha, D. F. Agterberg, J. Schmalian, N. P. Butch, J. Paglione, and A. Kapitulnik, Interplay between magnetism and superconductivity in UTe_2, Phys. Rev. B **105**, 024521 (2022).

[24] L. Jiao, Z. Wang, S. Ran, Jorge O. Rodriguez, M. Sigrist, Z. Wang, N. P. Butch, and V. Madhavan, Chiral superconductivity in heavy-fermion metal UTe_2, Nature (London) **579**, 523 (2020).

[25] A. Aishwarya, J. May-Mann, A. Raghavan, L. Nie, M. Romanelli, S. Ran, S. R. Saha, J. Paglione, N. P. Butch, E. Fradkin, and V. Madhavan, Magnetic-field sensitive charge density wave orders in the superconducting phase of UTe_2, Nature (London) **618**, 928 (2023).

[26] D. Aoki, J.-P. Brison, J. Flouquet, K. Ishida, G. Knebel, Y. Tokunaga, and Y. Yanase, Unconventional superconductivity in UTe_2, J. Phys.: Condens. Matter **34**, 243002 (2022).

[27] T. Metz, S. Bae, S. Ran, I. Liu, Y. S. Eo, W. T. Fuhrman, D. F. Agterberg, S. M. Anlage, N. P. Butch, and J. Paglione, Point node gap structure of spin-triplet superconductor UTe_2, Phys. Rev. B **100**, 220504(R) (2019).

[28] S. Kittaka, Y. Shimizu, T. Sakakibara, A. Nakamura, D. Li, Y. Homma, F. Honda, D. Aoki, and K. Machida, Orientation of point nodes and nonunitary triplet pairing tuned by the easy-axis magnetization in UTe_2, Phys. Rev. Res. **2**, 032014(R) (2020).

[29] K. Ishihara, M. Roppongi, M. Kobayashi, Y. Mizukami, H. Sakai, Y. Haga, K. Hashimoto, and T. Shibauchi, Chiral superconductivity in UTe_2 probed by anisotropic low-energy excitations, Nat. Commun. **14**, 2966 (2023).

[30] There exist two counter experiments to negate the claims: As for the polar Kerr effect, see M. O. Ajeesh, M. Bordelon, C. Girod, S. Mishra, F. Ronning, E. D. Bauer, B. Maiorov, J. D. Thompson, P. F. S. Rosa, and S. M. Thomas, The fate of time-reversal symmetry breaking in UTe_2, Phys. Rev. X **13**, 041019 (2023); As for the gap structure, see S. Suetsugu, M. Shimomura, M. Kamimura, T. Asaba, H. Asaeda, Y. Kosuge, Y. Sekino, S. Ikemori, Y. Kasahara, Y. Kohsaka *et al.*, Fully gapped pairing state in spin-triplet superconductor UTe_2, Science Adv. **10**, eadk3772 (2024).
[31] K. Machida and T. Ohmi, Phenomenological theory of ferromagnetic superconductivity, Phys. Rev. Lett. **86**, 850 (2001).
[32] K. Machida, Theory of Spin-polarized Superconductors–An Analogue of Superfluid ^{3}He A-phase–, J. Phys. Soc. Jpn. **89**, 033702 (2020).
[33] K. Machida, Notes on multiple superconducting phases in UTe_2 –third transition–, J. Phys. Soc. Jpn. **89**, 065001 (2020).
[34] K. Machida, Nonunitary triplet superconductivity tuned by field-controlled magnetization: URhGe, UCoGe, and UTe_2, Phys. Rev. B **104**, 014514 (2021).
[35] K. Machida, Violation of the orbital depairing limit in a nonunitary state: High-field phase in the heavy fermion superconductor UTe_2, Phys. Rev. B **107**, 224512 (2023).
[36] K. Machida, Theoretical studies on off-axis phase diagrams and Knight shifts in UTe_2: Tetra-critical point, d-vector rotation, and multiple phases, J. Low Temp. Phys. (2024), doi:10.1007/s10909-024-03181-3.
[37] Y. Tsutsumi, M. Ishikawa, T. Kawakami, T. Mizushima, M. Sato, M. Ichioka, and K. Machida, UPt_3 as a topological crystalline superconductor, J. Phys. Soc. Jpn. **82**, 113707 (2013).
[38] G. Eilenberger, Transformation of Gorkov's equation for type II superconductors into transport-like equations, Z. Phys. **214**, 195 (1968).
[39] N. Schopohl, Eilenberger equations for rotating superfluid ^{3}He and calculation of the upper critical angular velocity Ω_{c2}, J. Low Temp. Phys. **41**, 409 (1980).
[40] J. W. Serene and D. Rainer, The quasiclassical approach to superfluid ^{3}He, Phys. Rep. **101**, 221 (1983).
[41] M. Fogelström and J. Kurkijärvi, Quasiclassical theory of vortices in ^{3}He-B, J. Low Temp. Phys. **98**, 195 (1995).
[42] J. A. Sauls and M. Eschrig, Vortices in chiral, spin-triplet superconductors and superfluids, New J. Phys. **11**, 075008 (2009).
[43] Y. Nagato, K. Nagai, and J. Hara, Theory of the andreev reflection and the density of states in proximity contact normal-superconducting infinite double-layer, J. Low Temp. Phys. **93**, 33 (1993).
[44] N. Schopohl and K. Maki, Quasiparticle spectrum around a vortex line in a d-wave superconductor, Phys. Rev. B **52**, 490 (1995).
[45] M. Ichioka, N. Hayashi, and K. Machida, Local density of states in the vortex lattice in a type-II superconductor, Phys. Rev. B **55**, 6565 (1997).
[46] M. Ichioka, A. Hasegawa, and K. Machida, Field dependence of the vortex structure in d-wave and s-wave superconductors, Phys. Rev. B **59**, 8902 (1999).
[47] M. Ichioka, A. Hasegawa, and K. Machida, Vortex lattice effects on low-energy excitations in d-wave and s-wave superconductors, Phys. Rev. B **59**, 184 (1999).
[48] See Supplemental Material at http://link.aps.org/supplemental/10.1103/PhysRevB.110.L060507 for additional information, which includes Refs. [54–59].
[49] A. J. Leggett, A theoretical description of the new phases of liquid ^{3}He, Rev. Mod. Phys. **47**, 331 (1975).
[50] N. Nagaosa and Y. Tokura, Topological properties and dynamics of magnetic skyrmions, Nat. Nanotech. **8**, 899 (2013).
[51] Ashley M Cook, Topological skyrmion phases of matter, J. Phys.: Condens. Matter **35**, 184001 (2023).
[52] J. Sonier, J. Brewer, and R. F. Kiefl, μSR studies of the vortex state in type-II superconductors, Rev. Mod. Phys. **72**, 769 (2000).
[53] N. Read and D. Green, Paired states of fermions in two dimensions with breaking of parity and time-reversal symmetries and the fractional quantum Hall effect, Phys. Rev. B **61**, 10267 (2000).
[54] Jeffrey C. Y. Teo and C. L. Kane, Topological defects and gapless modes in insulators and superconductors, Phys. Rev. B **82**, 115120 (2010).
[55] M. Sato, Y. Tanaka, K. Yada, and T. Yokoyama, Topology of Andreev bound states with flat dispersion, Phys. Rev. B **83**, 224511 (2011).
[56] K. Shiozaki and M. Sato, Topology of crystalline insulators and superconductors, Phys. Rev. B **90**, 165114 (2014).
[57] A. P. Schnyder, S. Ryu, A. Furusaki, and Andreas W. W. Ludwig, Classification of topological insulators and superconductors in three spatial dimensions, Phys. Rev. B **78**, 195125 (2008).
[58] S. Ryu, A. P. Schnyder, A. Furusaki, and Andreas W. W. Ludwig, Topological insulators and superconductors: tenfold way and dimensional hierarchy, New J. Phys. **12**, 065010 (2010).
[59] M. Sato and S. Fujimoto, Topological phases of noncentrosymmetric superconductors: Edge states, Majorana fermions, and non-Abelian statistics, Phys. Rev. B **79**, 094504 (2009).